

Energetics of lateral eddy diffusion/advection: Part I. Thermodynamics and energetics of vertical eddy diffusion

HUANG Rui Xin¹*

¹ Department of Physical Oceanography, Woods Hole Oceanographic Institution, Woods Hole 02543-1050, USA

Received 30 August 2013; accepted 17 December 2013

©The Chinese Society of Oceanography and Springer-Verlag Berlin Heidelberg 2014

Abstract

Two important nonlinear properties of seawater thermodynamics linked to changes of water density, cabbeling and elasticity (compressibility), are discussed. Eddy diffusion and advection lead to changes in density; as a result, gravitational potential energy of the system is changed. Therefore, cabbeling and elasticity play key roles in the energetics of lateral eddy diffusion and advection. Vertical eddy diffusion is one of the key elements in the mechanical energy balance of the global oceans. Vertical eddy diffusion can be conceptually separated into two steps: stirring and subscale diffusion. Vertical eddy stirring pushes cold/dense water upward and warm/light water downward; thus, gravitational potential energy is increased. During the second steps, water masses from different places mix through subscale diffusion, and water density is increased due to cabbeling. Using WOA01 climatology and assuming the vertical eddy diffusivity is equal to a constant value of $2 \times 10^3 \text{ Pa}^2/\text{s}$, the total amount of gravitational potential energy increase due to vertical stirring in the world oceans is estimated at 263 GW. Cabbeling associated with vertical subscale diffusion is a sink of gravitational potential energy, and the total value of energy lost is estimated at 73 GW. Therefore, the net source of gravitational potential energy due to vertical eddy diffusion for the world oceans is estimated at 189 GW.

Key words: cabbeling, compressibility, elasticity, energetics of vertical eddy diffusion, gravitational potential energy, parameterization of eddy diffusion

Citation: Huang Rui Xin. 2014. Energetics of lateral eddy diffusion/advection: Part I. Thermodynamics and energetics of vertical eddy diffusion. Acta Oceanologica Sinica, 33(3): 1–18, doi: 10.1007/s13131-014-0409-6

1 Introduction

Oceanic circulation is a major component of the climate system on the Earth. With the advance of science and technology, numerical models of the oceanic general circulation become a more and more important tool in simulating and predicting the oceanic environment. Oceanic general circulation is commonly described by one set of primitive equations, including continuity equation, momentum equations and tracer equations. This set of equation is very complicated; thus, numerical models have been developed in order to find solutions for these equations subject to external forcing and boundary conditions. Oceanic general circulation is essentially a turbulent system, involving motions in broad temporal and spatial scales. As such, no numerical model can resolve motions on all spatial and temporal scales. Turbulent motions with spatial scales smaller than the grid size have to be parameterized. The final goal of numerical modeling of the oceanic general circulation is to simulate the oceanic circulation as accurately as possible. The success of a numerical model depends on many aspects of the models, such as the choice of coordinates, the discretization of the primitive equations and the parameterization of subgrid scale processes. Much progress took place over the past decades, and many numerical models are now running with horizontal resolution on the order of 1–10 km, and these models may be able to resolve meso-scale eddies.

1.1 Energetics of eddy diffusion and advection

Starting from the 1990s, a new paradigm about the energetics of thermohaline circulation in the world oceans emerged. According to the new paradigm, thermohaline circulation in the ocean is not a heat engine. Since the oceanic circulation is a dissipation system, in order to maintain quasi-steady circulation against internal friction and dissipation, external sources of mechanical energy are needed. Wind stress on the sea surface and tidal dissipation in the open ocean and are the primary sources of external mechanical energy (Munk and Wunsch, 1998; Huang, 1999). Since oceanic circulation takes place in the environment of gravity field, gravitational potential energy (GPE) is an important term direct linked to dynamics of the oceanic circulation. In particular, our focus in this study is the role of GPE source/sink related to eddy diffusion and advection.

Transport of tracers in the ocean consists of two components: advection and diffusion. Since the oceanic general circulation is essentially a turbulent system, the separation of tracer transport into these two components depends on the spatial scale in concern. On the finest scale, on the order of millimeter, tracer transport is regulated by advection and molecular diffusion. For scale larger than this level, tracer transport is regulated by advection and eddy diffusion. Since our concern is tracer transport of large scale circulation, with horizontal scale on the order of 1–10 km, diffusion discussed in this study is eddy diffusion.

*Corresponding author, E-mail: rhuang@whoi.edu

Advection of tracers is directly linked to the velocity field. Recent progress along this line includes the introduction of the eddy transport term, i.e., the advection term is separated into the mean flow transport and eddy transport. If we know the mean flow velocity, the contribution due to mean flow is relatively easy to calculate. Eddy transport parameterization has been discussed in many previous studies, and much progress has been reported; thus, this term is not the focus in this study.

On the other hand, diffusion (also called mixing) is directly linked to subgrid scale processes, including meso-scale and submeso-scale eddies, turbulence and internal waves. It is obvious that such small scale processes cannot be resolved in basin-scale numerical simulations. To incorporate the dynamical effects of these subscale processes into numerical models, different kinds of subgrid parameterization schemes have been postulated for momentum and tracers, including the momentum dissipation in the vertical and lateral directions and tracer diffusion (mixing) in the vertical and lateral directions. Tracer lateral diffusion in commonly used numerical models is treated basically in three ways: horizontal diffusion, isopycnal diffusion, and sigma diffusion. Since pressure surface is nearly horizontal, in this study we will use pressure coordinate instead of z -coordinates; thus, horizontal diffusion is actually diffusion along pressure surfaces. On the other hand, sigma diffusion means lateral diffusion along sigma surfaces.

These parameterizations are the most critical components for oceanic numerical modeling. Due to historical reasons, the parameterization of tracer diffusion had been treated as a subject disconnected with the balance of mechanical energy of the ocean. It is only within the last decade people came to realize that the ocean is not a heat engine and external sources of mechanical energy from wind and tides are required for sustaining the oceanic general circulation, including both the wind-driven circulation and thermohaline circulation. Over the past ten years, parameterization of vertical (diapycnal) eddy diffusion of tracers in the ocean based on mechanical energy available from tides and wind stress has advanced rapidly. Our focus in this study is on the lateral tracer diffusion and advection.

1.2 Lateral eddy diffusion and advection are important

It is obvious that subscale lateral diffusion of tracers is also a key component in oceanic numerical simulation. In particular, as we enter the era of eddy regime, simulating eddies accurately becomes one of the top priorities.

First, eddies contain more than 90% of the kinetic energy in the ocean. Eddies play a key role in transporting heat and freshwater and other tracers in the ocean. Thus, accurately simulating eddies is of vital importance for the description of the oceanic general circulation and the associated cycles of carbon and nutrients.

Second, eddy-eddy interaction is the critically important part of the oceanic dynamics. Eddy-eddy interaction is primarily through lateral processes; thus, accurate simulating lateral diffusion and advection is very desirable in oceanic circulation models.

Third, eddies decay primarily through lateral processes, with the vertical processes play a secondary role only. As we entering the regime of submesoscale eddy, accurately resolving fine structure in the lateral direction, such as fronts and filaments, become more and more important.

It is clear that without accurately resolving eddy motions,

numerical simulation about the ocean will not be able to provide us with the right information. Thus far, much effort has been focused on the parameterization of vertical eddy diffusion. On the other hand, lateral processes are as important as the vertical processes; however, the parameterization of lateral processes in the ocean has not received adequate attention up till now and progress along this line has been slow.

In fact, over the past several decades, the common practice of lateral diffusion of tracers in the ocean evolved; however, many aspects of lateral diffusion remain nearly unchanged. There are many ways of simulating the lateral spreading of tracer through advection and diffusion. First, different vertical coordinates have been used, such as the geopotential coordinate (often called z -coordinate), the isopycnal coordinate, or the sigma coordinate. Lateral diffusion in these coordinates can be parameterized in many different ways, such as Laplacian diffusion, bi-harmonic diffusion, the Smagriniski scheme and other schemes. In addition, the diffusivity adapted in these schemes is commonly assumed to be homogeneous and isotropic in the world oceans. Furthermore, the diffusivity is treated as an arbitrary constant which the modeler can choose almost arbitrarily. In fact, there is no commonly accepted criterion to judge whether the lateral diffusion scheme and the corresponding diffusivity have been chosen appropriately. To my best knowledge no paper linking lateral diffusion to GPE has ever been published. We will first reexamine some of the thermodynamic properties and physical processes which can be used to describe thermohaline circulation and variability in the world oceans, including cabbeling and thermobaricity.

The terminology used in this study is as follows. Since our focus in this study is phenomena on horizontal scale on the order of 1–100 km (the so-called meso-scale or the submeso-scale), much larger than the molecular scale, we are dealing with eddy diffusion, not molecular diffusion. Hence, we will conceptually separate eddy diffusion into two stages: stirring and subscale diffusion. The first stage, stirring, will be considered as adiabatic in this study. The second stage involves subscale process of diffusion driven by eddies of subgrid scales, turbulence and internal waves; thus, processes involved for individual water parcels in the second stage are not adiabatic.

According to the common wisdom, water parcels moving along isopycnal surfaces or along the neutral surface (NS) do not experience buoyancy force. This is equivalent to the statement that isopycnal stirring is free of buoyancy work; consequently, there is no GPE change in the system. We will examine the GPE change due to lateral stirring along lateral direction in Part II (Huang, 2014a). Careful analysis shows that due to the thermobaric effect, stirring, or exchanging water masses, along quasi-horizontal surfaces (horizontal, isopycnal or sigma) is associated with changes of GPE in the mean state. In addition, in the second stage, subscale diffusion, cabbeling associated with subscale turbulent diffusion can release GPE from the mean state. We postulate that meso-scale thermohaline perturbations on potential density surface (PDS) (or quasi-NS) may grow with GPE released through isopycnal stirring and cabbeling. This is a new kind of meso-scale instability. Although this instability may be linked to the well-known instabilities associated with double diffusion and the baroclinic instability; it is also quite different from these two well-known types of instability.

In early days of ocean modeling, due to the limitation of computer power, lateral eddy diffusivity in the model run was

set to rather high values, on the order of 10^6 m²/s (or even higher); such high values were needed to suppress numerical instability. With the rapid progress in computer technology and numerical modeling, models with resolution fine enough to resolve meso-scale eddies become more and more accessible. With the increasing of computer power, models running on fine resolution on the order of 1–10 km do not require such artificially high diffusivity. In fact, many high resolution models are now running with very low (or even zero) lateral diffusivity. Because the horizontal resolution of such models is or the order of tenths of deformation radius, they are often called eddy-resolving model; many people believe that such models can really resolve eddy-eddy interaction, at least for the low and middle latitudes. However, *in-situ* observations over the past half century indicate that lateral diffusion in the ocean is finite, but not zero; hence, setting the lateral eddy diffusivity to zero in these models implies that the models are not working properly. As will be shown in this study, models based on Eulerian coordinates can introduce strong artificial diffusion through the lateral advection terms. Thus, results obtained from such models may not be accurate for horizontal scale equal to the model resolution. If reliable results from such models are desirable, people may have to trust properties on the order of 3–5 times of the model resolution. Of course, exactly how to evaluate the potential errors and artifacts in numerical simulations have always been a challenging subject.

Whether the model output is reliable must be evaluated with some acceptable criteria. In particular, whether lateral advection/diffusion is simulated accurately in an oceanic general circulation model can be examined from different angles. The most objective criterion is to compare the model outputs with observations. This approach is, unfortunately, of limited use because we do not have adequate data which can be used for comparison. In particular, with the model resolution entering eddy-resolving regime, there is simply no data with enough spatial and temporal resolution to be compared with the model outputs.

As an alternative, we will use the GPE source/sink associated with the lateral advection/diffusion as an objective to be compared with the potential source of mechanical energy in the world oceans. First, we will estimate the potential mechanical energy available for sustaining lateral advection/diffusion; i.e., we will set an upper limit for the source/sink terms. Second, we will estimate the GPE source/sink associated with lateral advection/diffusion simulated in different oceanic general circulation models. If the source/sink associated with such dynamical processes in a model is much larger than the upper limit, such simulation in the ocean model is questionable.

To begin with, we review the mechanical energy balance in the world oceans. According to the new paradigm, the oceanic circulation is not a heat engine, and its circulation is maintained by external sources of mechanical energy (Munk and Wunsch, 1998; Huang, 1999, 2010). Unfortunately, there is no reliable and accurate estimate about the mechanical energy balance for the world oceans. The current state of art of the mechanical energy diagram is shown in Fig. 1. This is a rough diagram, and most terms are accurate within a factor of 2 only. The most important terms are as follows.

The largest item in this diagram is the wind energy input into surface waves. A preliminary estimate of this term is about 60 TW (1TW=10¹² Watts), although another independent estimate puts its value at 68 TW. However, it is believed that most of this energy is dissipated within the surface wave boundary layer and the mixed layer, with very little energy left and being carried down into the subsurface layers. The downward transform of mechanical energy from the surface waves is mostly in the form of near inertial waves; the pathways and the exact amount of this downward energy flux remain unknown.

The second largest item is wind energy input into the surface Ekman layer, and a rough estimate of this term is about 3.1 TW. Once again, this mechanical energy is mostly dissipated within the mixed layer, with only a small fraction left behind and being carried to the depth below the base of the Ekman layer. In particular, a small part of this energy may exist in the form of

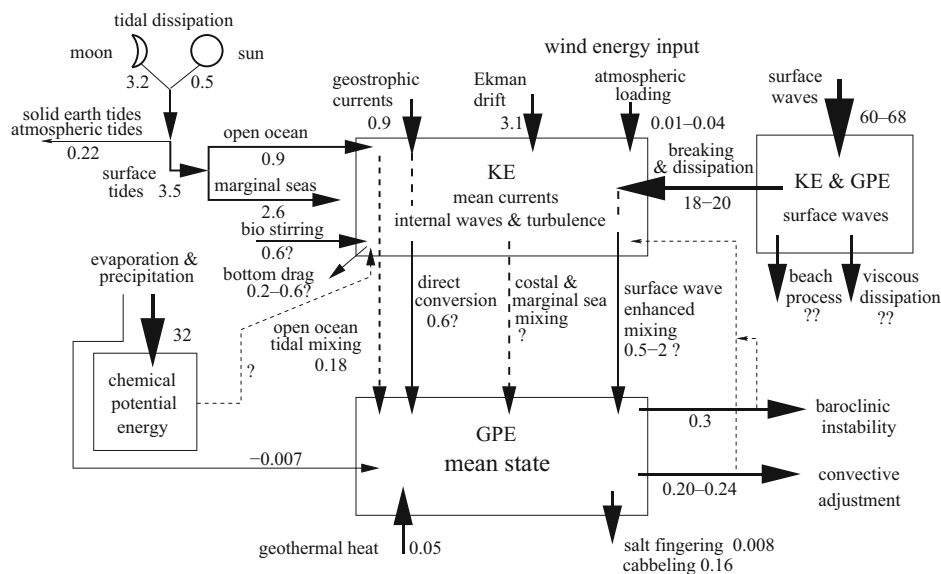


Fig. 1. The most updated mechanical energy diagram for the world oceans (in unit of TW), modified from Huang (2010). The GPE due to cabelling associated with vertical and isopycnal diffusion is based on the results from this study.

near inertial waves, which can penetrate through the based on the mixed layer and thus affect mixing in the subsurface ocean. However, the exact amount of such energy remains debatable at this time.

There is a huge amount of chemical energy input into the upper ocean (32 TW). However, it is likely that most of this energy is dissipated within the thin surface boundary layer. In addition, the rest of this chemical energy is primarily contributed to small scale diffusion only, and its contribution to large-scale circulation remains obscure.

For large-scale ocean circulation, mechanical energy from tidal dissipation is an important source. Tidal dissipation in the open ocean is about 0.7–0.9 TW (Munk and Wunsch, 1998). Assuming a conversion coefficient of 20%, it gives rise to a GPE source of 0.18 TW. As will be shown in Section 3, this amount of GPE is equal to the GPE generated by vertical eddy diffusion in the world oceans, assuming a vertical diffusivity of $0.2 \times 10^{-4} \text{ m}^2/\text{s}$. This source of mechanical energy is probably one of the most important sources of energy sustaining vertical/lateral diffusion in the subsurface ocean.

From the upper surface, the wind stress energy input to the surface geostrophic current is about 0.9 TW. Most of this wind energy input is believed to be used to sustain the baroclinic instability (about 0.3 TW). In addition, convective adjustment taken place at high latitudes may require 0.20–0.24 TW. Finally, the bottom drag can be a large sink for mechanical energy, and the current estimate is about 0.2–0.6 TW. This number is with a great uncertainty; however, this is the state of art of mechanical energy balance in the world oceans. Cabbeling is also an important sink of mechanical energy. As will be discussed in this study energy sink due to cabbeling associated with vertical diffusion and lateral diffusion in the world oceans is estimated at 0.073 and 0.09 TW respectively, and the sum is 0.16 TW.

Note that although in many previous studies, mechanical energy balance was mostly confined to the vertical (diapycnal) diffusion; we will also explore the potential role of mechanical energy in lateral eddy diffusion. Given the estimate of all these important sinks, the potential sink associated with lateral advection and diffusion seems very small. The exact amount of such energy remains unexplored. In this study we will tentatively put the upper limit as 0.05–0.1 TW. Comparing with the 0.18 TW associated with vertical diffusion, this is a sizeable amount of energy. Therefore, in our analysis below, any results of global integrated energy source/sink associated with lateral advection/diffusion that requires mechanical energy larger than 0.1 TW is consider to be questionable, and the corresponding choice of vertical coordinates and parameterization of lateral eddy diffusion and advection in the model is considered unphysical and should be avoided.

1.3 Data used in our analysis

Although oceanographic data of temperature and salinity are often collected in terms of pressure coordinate, most climatological datasets use the z -coordinate to form gridded data. Such a practice is unnecessary and inconvenient for application because the equation of state for seawater is defined in terms of pressure. In this study, thus, we convert the standard z -levels in the WOA01 data (Conkright et al., 2002) into the corresponding pressure levels, using the standard converting subroutine. Note that the equivalent pressure levels obtained depend on latitude; therefore, we further interpolate this data into a gridded dataset

with standard pressure levels of 0, 10, 20, 30, 50, 75, 100, 125, 150, 200, 250, 300, 400, 500, 600, 700, 800, 900, 1 000, 1 100, 1 200, 1 300, 1 400, 1 500, 1 750, 2 000, 2 500, 3 000, 3 500, 4 000, 4 500, 5 000 and 5 500 (10^4 Pa). This will be called the converted WOA01 data.

The goal of this study is to quantify GPE source/sink associated with lateral diffusion and advection. In particular, we will examine potential errors associated with lateral advection terms in the Eulerian coordinates. In an early study, Griffies et al. (2000) discussed the artificial diapycnal diffusion associated with the advection terms in z -coordinate model. However, many important issues related to the advection in Eulerian coordinates remain unexplored. In order to estimate the potential GPE source/sink due to stirring/cabbeling associated with lateral advection, we need information about the velocity field. There can be different approaches.

The first approach is to run models based on three different vertical coordinates, the z -coordinates (or the pressure coordinates), the isopycnal coordinates, and the sigma coordinates (or the so called s -coordinates). A close examination reveals that such an approach may be questionable. Models based on these coordinates involved different discretization in the vertical and lateral directions and different parameterizations of subscale processes. Consequently, results obtained from these models (including temperature, salinity and velocity distribution) can be quite different, and comparison between these models may not give clear explanation of the physics hidden behind.

In order to do the comparison in a clean way, we postulate the second approach as follows. Using a climatologic mean state of ocean circulation produced from a numerical model, we can generate a dataset for the world ocean, including the temperature, salinity and velocity distribution. Our choice is the SODA data, which has been used in many previous studies, and there is a 50 year dataset available (SODA 2.1.6; Carton and Giese, 2008). From this 50 year annual mean field we generated the 50-year mean climatological state of the world ocean circulation. This dataset will be called the SODA data in this study, unless specifically explained otherwise.

Since the SODA data is based on the z -coordinates, we have temperature, salinity and horizontal velocity on the regular z -grid, which can be directly used in the GPE source/sink analysis for a z -coordinates model.

The GPE source/sink for isopycnal diffusion and advection will be discussed in Part III (Huang, 2014b). For the isopycnal coordinates, we use the same spatial grid taken from the z -coordinates and the only thing we need to do is to project the temperature, salinity and horizontal velocity from z -coordinates in the original dataset onto the isopycnal coordinates. We adapt the common practice in the model community as follows. The isopycnal slope is defined by the mean stratification between two adjacent grid points. Using interpolation between grid points, we generate the corresponding temperature and salinity on the adjacent points which are need for the GPE calculation in isopycnal coordinates. In theory, we may need to project the horizontal velocity onto the isopycnal surfaces as well. However, in most cases, the slope of the isopycnal surface is quite small, on the order of 1/100 or less. Thus, the lateral velocity on the isopycnal surface obtained from such projection is practically the same as the horizontal velocity on the z -coordinates before projection. The potential errors involved in such assumption are on the order of no more than a few percentages.

As will be shown in the subsequent calculations in this study, the GPE source/sink diagnosed from different coordinates differs in their order of magnitude; therefore, such potentially small errors involved are acceptable.

For the sigma coordinates, we first generate the corresponding sigma grid for the world oceans, and the technical detail will be explained in Part IV (Huang, 2014c) where GPE source/sink in sigma coordinates will be discussed in details. The corresponding temperature and salinity on this sigma grid is generated by projecting the temperature and salinity from the original z -grid in SODA data onto the sigma coordinates. In theory, we may need to project the horizontal velocity onto the sigma coordinates as well. However, in most cases, the slope of the sigma surface is quite small, on the order of 1/100 or less. Hence, the lateral velocity on the sigma surface obtained from such projection is practically the same as the horizontal velocity without projection. Thus, adapting the same approach used in the case of isopycnal coordinates we will simply use the horizontal velocity taken from the original 50-year mean SODA data and project it onto the sigma grid, without considering the effect of sigma surface slope on the lateral velocity. As will be shown in the subsequent calculations in this study, the GPE source/sink diagnosed from different coordinates differs in their order of magnitude; thus, such potential small errors involved are acceptable.

This Part I of our study is organized as follows. In Section 2, two important seawater thermodynamic properties are discussed, including cabbeling and compressibility. We introduce a new term, elasticity, which can be used to describe the GPE change due to lateral eddy stirring. In Section 3, we examine GPE changes due to vertical eddy diffusion, and this GPE change can be used as a reference value for the GPE changes due to lateral eddy diffusion and advection.

2 Cabbeling and elasticity

The equation of state of sea water is nonlinear. Such nonlinearity manifests in different forms. Two of the phenomena associated with the nonlinearity are cabbeling and elasticity (compressibility), which is highly relevant to energetics of eddy diffusion and advection in the ocean. Discussion here will be focused on these two subjects.

As the common practice in physical oceanography, seawater is treated as a two-component thermodynamic system, and its thermodynamic state can be uniquely determined in terms of three independent variables, including temperature, salinity and pressure. Furthermore, oceanic circulation is often examined in terms of property distribution on thermodynamic surfaces (pressure surface, potential density surface, etc.); on such surfaces the thermodynamics of seawater can be described in terms of two independent variables. One of the most important and commonly used thermodynamic variables is density. Density distribution in the vertical direction controls the stability of the water column, and its horizontal distribution is directly linked to the horizontal pressure gradient and thus the circulation in the ocean.

In addition to density, we need another thermodynamic variable to provide the additional information for defining the thermodynamic state of the system. Ideally, the other variable should provide the rest of the thermodynamic information with the least amount of overlapping with density, i.e., the most desirable thermodynamic variable complementary to

density should be “orthogonal” or “perpendicular” to density isopleths in the (T, S) diagram, as discussed in many previous studies, such as Stommel (1962), Veronis (1972), Munk (1981), and Flament (2002). A new terminology, spicity, which definition meets the most desirable properties of this variable, was recently reintroduced by Huang (2011).

There are two well-known aspects of the nonlinearity of the equation of seawater, including cabbeling and thermobaric effect. Cabbeling is a process taking place when two water parcels with different temperature and salinity mix. Due to the nonlinearity of state of seawater the density of the final product is higher than the mean density of the parent parcels; as a result, GPE is released. Energy release due to cabbeling is well known. Gill (1973) studied the convective instability associated with cabbeling. Fofonoff (1998, 2001) studied the energy release associated with vertical diffusion or turbulent exchange of water parcels in a vertical column.

Thermobaric effect is named after a special property of seawater: cold and fresh water is more compressible than warm and salty water. One of the most important implications of thermobaricity is directly linked to the bottom water formation. At the sea surface, Mediterranean Outflow Water, characterized as warm and salty, has the highest density among all the source waters for the deep ocean. In particular, on the sea surface it is heavier than the outflow from the Filchner Ice Shelf. However, the later is relatively fresh and cold. Due to the thermobaric effect, it is more compressible than that of Mediterranean Outflow Water. Thus, it can become the heaviest water and sinks to the bottom of the world oceans. On the other hand, Mediterranean Outflow Water is relatively warm and saltier, so it is less compressible; consequently, it can sink to the level of 1.5 km only. Note that entrainment associated with the overflow also contributes to the determination of the density of the overflow product; however, thermobaric effect is of utmost importance (Price and Baringer, 1994; Huang, 2010).

The study of thermohaline circulation can be carried out by examining the distribution of thermodynamic variables on surfaces defined by a constant thermodynamic variable, such as potential density. Although spicity can be used for such a purpose, its application may be limited to double diffusive processes. Until now, the study of double diffusion has been mostly focused on salt finger and diffusive layering or thermohaline intrusions, which are mostly confined to the vertical planes and with typically horizontal scale smaller than a few kilometers, as discussed in many previous studies (Ruddick and Kerr, 2003; Ruddick and Richards, 2003).

On the other hand, most basin-scale oceanic numerical models have been running with horizontal resolution on the order of 10–100 km. Quasi-horizontal (horizontal, isopycnal or along-sigma surface) diffusion of tracers is a key component of such numerical simulations. However, the stability of quasi-horizontal thermohaline perturbations on such horizontal scales has not been explored thoroughly. Thus, one of our goals in this study is to explore whether such horizontal thermohaline perturbations can grow supported by GPE released from the mean state. As will be shown in this study, the thermobaricity of seawater plays an important role in regulating the instability of such thermohaline perturbations.

In summary, most previous studies on thermohaline processes in the ocean were focused on dynamical processes taking place in the vertical direction, and with horizontal scale on

the order from 1–100 m. The focus of this study is the instability of the quasi-horizontal perturbations, which has the horizontal scale of the most energetic eddies in the ocean, i.e., scale of 1–100 km. We postulate that during exchanging and subscale turbulent diffusion of water parcels along isopycnal surfaces, GPE can be released due to the thermobaric and cabbeling effects. To describe the instability of meso-scale quasi-horizontal perturbations a new terminology, elasticity (the compressibility of seawater) is introduced. The combination of elasticity and cabbeling is a convenient tool in describing the energetics of meso-scale lateral thermohaline perturbations.

2.1 Cabbeling

2.1.1 Basic concept of cabbeling

Cabbeling is a classical concept in physical oceanography, and a concise description is included here. Cabbeling was first discussed in oceanography almost 100 years ago. This word was introduced to describe the following phenomenon: when two water parcels are mixed, the density of the mixed product is always higher than the mean of the parent water parcels. A simple case is illustrated in Fig. 2. At sea surface two water parcels with equal mass have exactly the same density, but different temperature and salinity. After these two parcels are mixed, the final product has a density slightly higher than the density of the original parcels.

Note that the heat capacity of sea water is not constant. According to Feistel (1993), the heat capacity under constant pressure of the cold parcel (0°C for temperature and 34 for salinity)

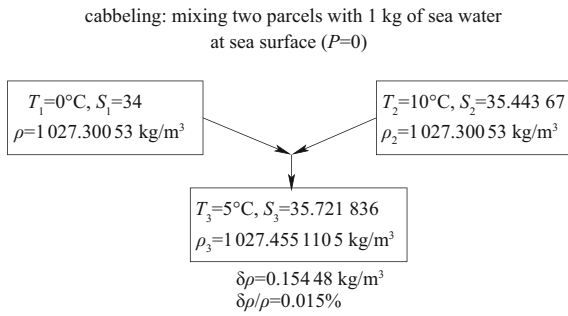


Fig.2. An example of water parcel mixing leading to cabbeling. For simplicity, we assume that mixing takes place at the sea surface.

is 3992.6 J/kg·K⁻¹, slightly larger than the value of 3989.4 J/kg·K⁻¹ for the warm parcel (10°C for temperature and 34.443.67 for salinity). As a result, the final product after mixing should have a temperature slightly lower than 5°C, and corresponding density of the mixed water parcel should be increased slightly. However, such a correction is rather small, and we will assume that heat capacity under constant pressure is constant and omit the small correction to the cabbeling calculation in this study.

For the general case, we assume that two water parcels with equal mass are under the same pressure; their initial temperature and salinity are

$$\begin{aligned} T_1 &= T + \Delta T, T_2 = T - \Delta T; \\ S_1 &= S + \Delta S, S_2 = S - \Delta S. \end{aligned} \quad (1)$$

In addition, we also assume that specific heat is approximately constant. After these water parcels mix, the final temperature and salinity is T and S . Using the Taylor expansion, the mean density of these two water parcels before subscale turbulent diffusion is

$$\begin{aligned} \bar{\rho}_{\text{initial}} &= 0.5(\rho_1 + \rho_2) \\ &= \rho_0 + 0.5(\rho_{TT}\Delta T^2 + \rho_{SS}\Delta S^2 + 2\rho_{ST}\Delta T\Delta S), \end{aligned} \quad (2)$$

where $\rho_0 = \rho_{\text{mixed}} = \rho(S, T, P)$ is the density after subscale turbulent diffusion. Hence, density change due to subscale turbulent diffusion is

$$\begin{aligned} \rho_{\text{mixed}} - \bar{\rho}_{\text{initial}} &= -0.5\rho_{TT}\Delta T^2 - 0.5\rho_{SS}\Delta S^2 - \rho_{ST}\Delta T\Delta S \\ &\approx -0.5\rho_{TT}\Delta T^2 > 0. \end{aligned} \quad (3)$$

As shown in Fig. 3, all second derivatives of density are negative

$$\rho_{TT} = -\bar{\rho}\alpha_T < 0; \quad \rho_{SS} < 0; \quad \rho_{ST} < 0. \quad (4)$$

Thus, the density anomaly induced by mixing is always positive, i.e., cabbeling in the ocean always leads to the formation of water parcels with higher density.

In general, density increase due to cabbeling is high for cold and fresh water (Fig. 4a). Temperature is the primary factor controlling the density increase due to cabbeling, and salinity plays a secondary role. In addition, density increase is high at

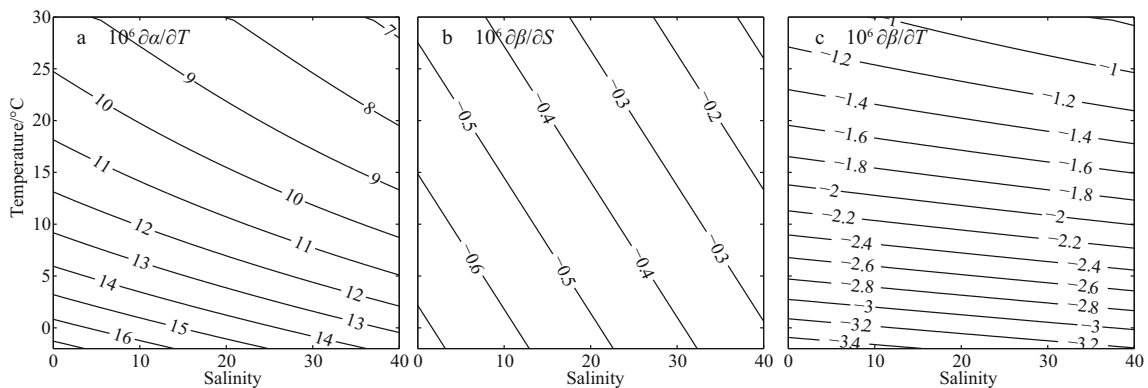


Fig.3. The second derivatives of density, under sea level pressure ($P=0$).

low pressure, but it is much lower under high pressure (Fig. 4b).

The most important factors regulating cabbeling are as follows. The first factor is the derivative of the thermal expansion coefficient, which is nearly constant for the temperature range below 5°C. The second factor is the strong temperature gradient associated with fronts, such as the Gulf Stream, Kuroshio and the Antarctic Circumpolar Current (ACC). In addition, because density is increased due to cabbeling, the whole water column above moves down and GPE of the mean state is reduced; energy release due to cabbeling can enhance small scale perturbations, such as turbulence. The amount of GPE released due to cabbeling is linearly proportional to the total mass of the water column above; thus, it is proportional to the *in-situ* pressure. These factors will be important ingredients controlled GPE release associated with lateral diffusion/advection discussed in this study.

2.1.2 *Anti-cabbeling associated with artificial mixing due to horizontal advection*

In general, mixing of water parcels always leads to cabbeling; however, due to the horizontal advection terms in the Eulerian coordinates, something equivalent to demixing (or separating) can happen in numerical models. The following simplified examples with water masses in three boxes (box 1, 2 and 0) are used to illustrate the basic idea.

A simple case is mixing of three water parcels with different

temperature (T_1, T_2, T_0), but the same salinity $S=35$, shown in Fig. 5. Before mixing, these water parcel's density can be calculated from the equation of state:

$$\rho_1 = \rho(S, T_1, p), \rho_2 = \rho(S, T_2, p), \rho_0 = \rho(S, T_0, p). \quad (5)$$

Mixing of these water parcels can be conceptually separated into two steps. First, when these three components are put together and the mixture stirred, the mean density of the mixture before the small scale diffusion sets in is

$$\bar{\rho} = (a\rho_1 + b\rho_2 + c\rho_0) / (a + b + c). \quad (6)$$

During the second phase of mixing, small scale diffusion takes place and the mixture acquires a new mean temperature

$$T = (aT_1 + bT_2 + cT_0) / (a + b + c). \quad (7)$$

Note that due to the nonlinearity of equation of the state, the final temperature is slightly different from the simple linearly weighted mean temperature defined above. However, such a correction is minor in general, and for simplicity we will use the simple formula in Eq. (7) and avoid the rather complicated calculation. The corresponding density of the final mixture is

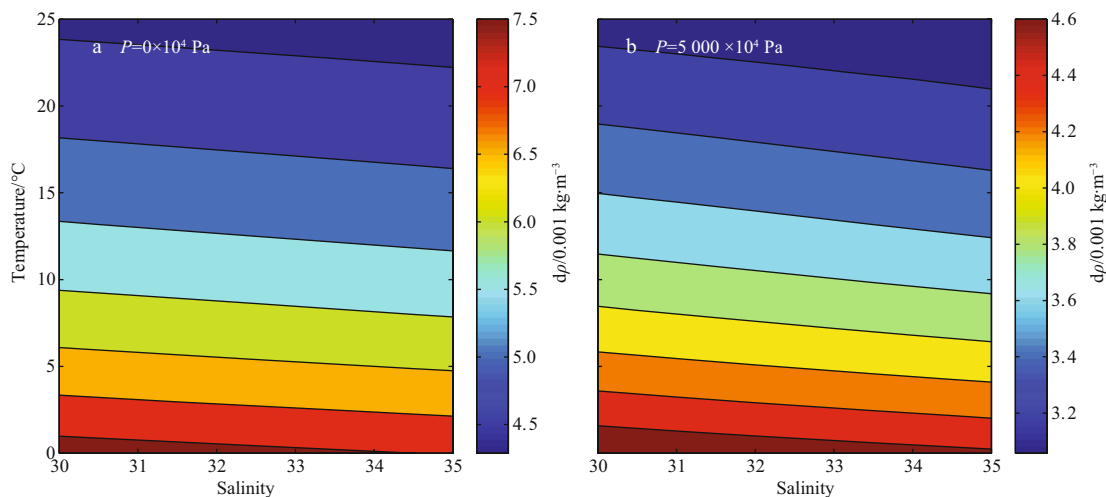


Fig.4. Cabbeling in the ocean: density increase due to mixing of two water parcels with $\Delta T = \pm 1^\circ\text{C}$, $\Delta S = \pm 0.25$.

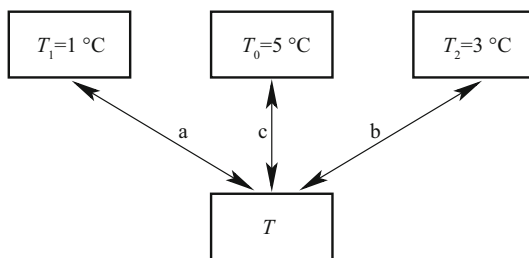


Fig.5. Sketch of mixing three water parcels with different temperature, where a, b and c are the mixing ratios. A positive value of a (or b and c) indicates that water flows into the mixer; a negative value indicates water leaves the mixer.

$$\rho_{\text{final}} = \rho_{\text{final}}(S, T, p).$$

We keep the mixing ratio $c \equiv 1$ (i.e., water always flows from box 0 to the mixer) and vary both a and b . In the case with both a and b are positive (i.e., water flows from boxes 1 and 2 into the mixer), the final mixture has a density higher than the mean density before the small scale diffusion, as shown in the left panel of Fig. 6.

On the other hand, if either a or b is negative (i.e., water leaves the mixer and flows into box 1 or 2), the final density can be smaller than the mean density before the final small scale diffusion, as shown in the right panel of Fig. 6. For example, if $a > 0$ and $b < 0$, it means water comes from box 1 and 0, and is exported to box 2. Water comes from box 1 and 0 is mixed together; however, water exported to box 2 means demixing, and the corresponding density decline is called anti-cabbeling.

From the physical point of view, mixing of water parcels always leads to increase of density, i.e., the cabbeling discussed in many previous studies. However, in numerical models based on central difference in the Eulerian coordinates, advection can lead to artificial demixing and anti-cabbeling. The artificial phenomena will be further discussed in this study. See Part II, III and IV (Huang, 2014a, b, c).

2.2 Elasticity

Thermohaline circulation is often studied through examining thermodynamic properties on PDSs or other similar surfaces. Since density is constant on such a surface, we need to find another thermodynamic variable, which is complementary to density. Spicity was introduced as such a tool in the study of thermohaline circulation, in particular the study of double diffusion. There is another thermodynamic property which can be used in a similar way. Seawater is slightly compressible, and the compressibility of seawater is not constant. In fact, cold and fresh water is more compressible than warm and salty water, and such a property is called the thermobaricity.

The compressibility under constant entropy and salinity is defined as

$$K_{\eta} = \frac{1}{\rho} \left(\frac{\partial \rho}{\partial p} \right)_{\eta, S} = \frac{1}{\rho c^2} (\text{Pa}^{-1}), \quad (8)$$

where $c = \sqrt{(\partial p / \partial \rho)_{\eta, S}}$ is the sound speed; compressibility in the world oceans is within the range of $(4.1-4.7) \times 10^{-10} \text{ Pa}^{-1}$.

For convenience we will introduce a term *elasticity*, which is defined as

$$E = 1000 \times 10^4 \text{ Pa} \cdot \rho K_{\eta} = \frac{1000 \times 10^4 \text{ Pa}}{c^2} \text{ kg/m}^3. \quad (9)$$

Thus, elasticity has the same unit as density. By definition, elasticity is the density increment due to $1000 \times 10^4 \text{ Pa}$ (very slightly smaller than 1000 m in depth) increase in pressure through an adiabatic and isohaline movement of a water parcel. Elasticity of seawater can be calculated with standard Matlab or FORTRAN codes currently used in the oceanographic community. We will use the following formula to calculate density increment due to change in pressure:

$$\delta \rho = E \delta p / 1000, \quad (10)$$

where δp is pressure change in the unit of 10^4 Pa , and density change is in the unit of kg/m^3 . Note that in fluid dynamics the Bulk Modulus Elasticity is defined as the reciprocal of the compressibility under constant entropy discussed above, i.e.,

$$E_i = -v \frac{dp}{dv} = \rho \frac{dp}{d\rho}. \quad (11)$$

The commonly used unit is Pa. In this study, we use elasticity E defined by Eq. (9).

Elasticity is an important thermodynamic variable regulating the thermohaline circulation. In general, elasticity can be defined as a function of *in-situ* temperature, salinity and pressure. However, one can also use the so-called potential elasticity, defined as a function of potential temperature referred to the specific reference pressure, salinity and *in-situ* pressure. In

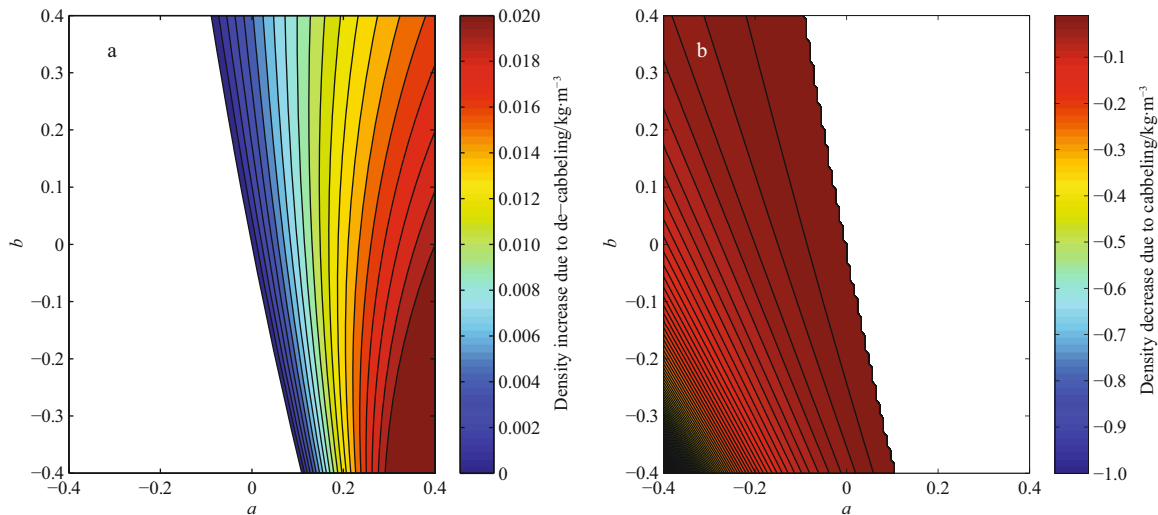


Fig.6. Density changes due to mixing or demixing of three water parcels with different temperature.

general, elasticity isopleths are not perpendicular to the density isopleths (Fig. 7). Nevertheless, elasticity can also provide information complementary to density. As will be further shown, gradient of elasticity on PDSs is closely linked to the source/sink of GPE associated with meso-scale thermohaline perturbations on such surfaces.

As shown in Fig. 7, for the practical range of temperature and salinity in oceanography, elasticity varies within the range of 4.1–4.7 kg/m³. It depends primarily on the temperature, with the salinity plays a secondary role. The most important point is that cold and fresh water is more compressible and thus has a high elasticity; while warm and salty water is less compressible and thus has a low elasticity. The difference in elasticity is an important factor regulating thermohaline circulation, including bottom/deep water formation. As will be shown shortly, the gradient of elasticity can also induce the instability of thermohaline perturbation on potential density surfaces.

2.3 Distribution of spicity and elasticity in the world oceans

As the first example, we show a meridional section of spicity and elasticity. Using the converted WOA01 data, the distribution of spicity and elasticity along 179.5°W are calculated and shown in Figs 8 and 9. These two maps share many similarities, especially in the upper ocean. Spicity is a thermodynamic variable indicating the most outstanding difference of water masses in the meridional section (Fig. 8). Typically, spicity has high positive values at low latitudes and high negative values at high latitudes; such features are directly linked to the warm/salty water at low and middle latitudes and the cold/fresh water at high latitudes. On the other hand, at low latitudes water with high temperature and salinity gives rise to low value of elasticity; but, at high latitudes water with low temperature and salinity gives rise to high value of elasticity (Fig. 9). As will be explained shortly, the strong gradient of elasticity is closely linked to the instability of thermohaline perturbations on quasi-horizontal surfaces.

Both spicity and elasticity are important thermodynamic properties of seawater, but they may reflect quite different aspects of thermodynamic property of water masses. Spicity is closely linked to the different roles of temperature and salinity

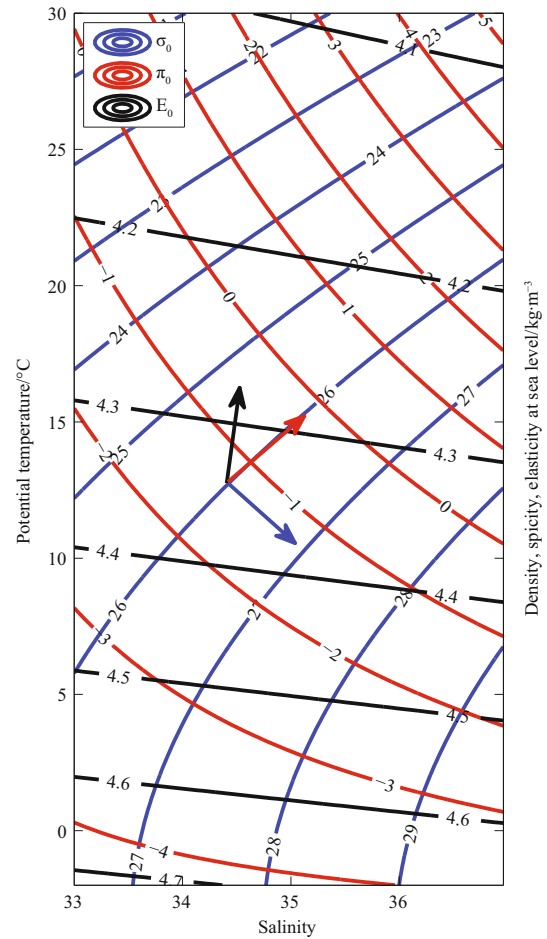


Fig.7. Potential density (blue curves), potential spicity (red curves), and potential elasticity (black lines) as functions of potential temperature and salinity, using the sea level pressure as the reference pressure; the arrows indicate the directions of the normal vectors perpendicular to the corresponding isopleths.

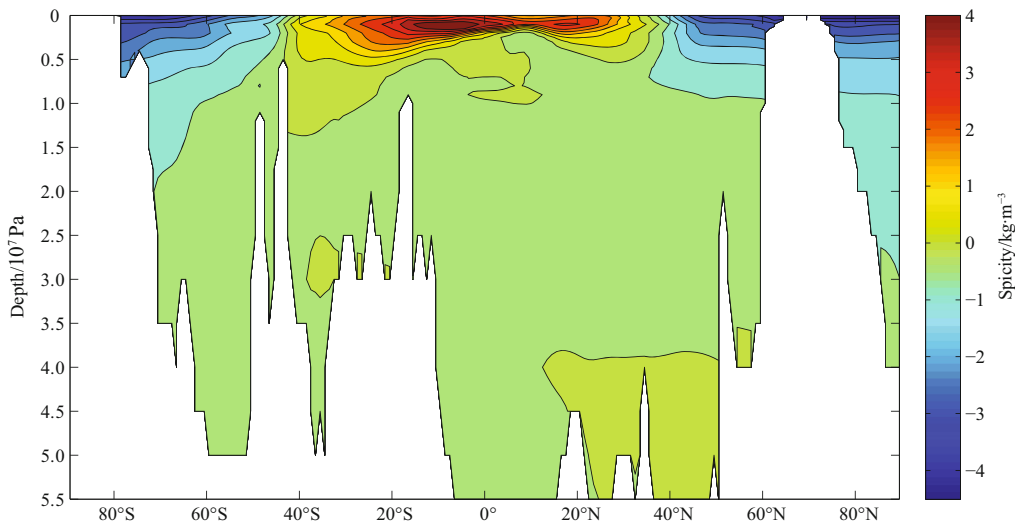


Fig.8. Spicity distribution along the 179.5°W section.

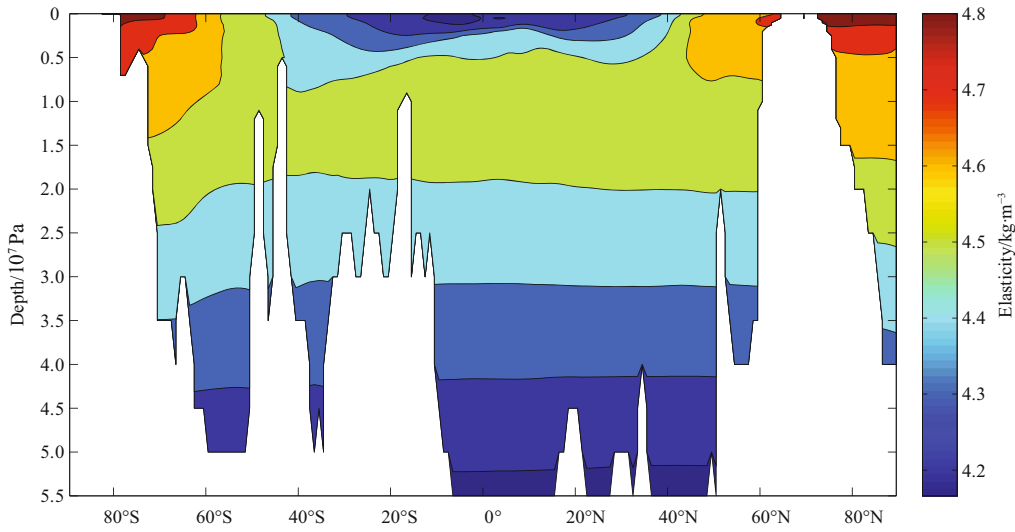


Fig.9. Elasticity distribution along the 179.5°W section.

in the thermohaline circulation, and such roles are directly connected to the different diffusivity of temperature and salinity for different length scales of motion. Therefore, spicity has been used as a very important index in the study of double diffusion, which is mostly focused on instability of the quasi-vertical perturbations, such as salt fingers and thermohaline interleaving and layering.

On the other hand, elasticity or thermobaricity is not directly linked to the difference in molecular diffusivity of temperature and salt. Instead, it may be linked to the instability of quasi-horizontal perturbations with scale on the order of 1–100 km; and this is our focus in this study.

In order to explore the physics of quasi-horizontal thermohaline perturbations we can plot the water mass property distributions on isopycnal surfaces. There are many possible choices for the isopycnal surface, including neutral surface (NS)

or potential density surface (PDS). Due to the nonlinear equation of state for seawater, no exact NS can be defined for the world oceans. As a result, there are only approximate NSs (Jackett and McDougall, 1997; Eden and Willebrand, 1999). Thus, we will use the other alternative, i.e., use the PDS. For the upper ocean, over the depth range of 0–1000×10⁴ Pa, the best choice is the potential density $\sigma_{0.5}$, which is defined using 500×10⁴ Pa as the reference pressure. The additional advantage of using a PDS is that potential density is a conserved quantity.

We will use PDS $\sigma_{0.5}=29.3 \text{ kg/m}^3$. This PDS intersects the main thermocline in the subtropical basins of both the North Pacific Ocean and North Atlantic Ocean at the depth range of 500×10⁴–800×10⁴ Pa (Fig. 10). In the Southern Hemisphere, it is slightly deeper, in particular in the Indian Ocean sector. This PDS also intersects the subpolar basins and strong fronts of ACC.

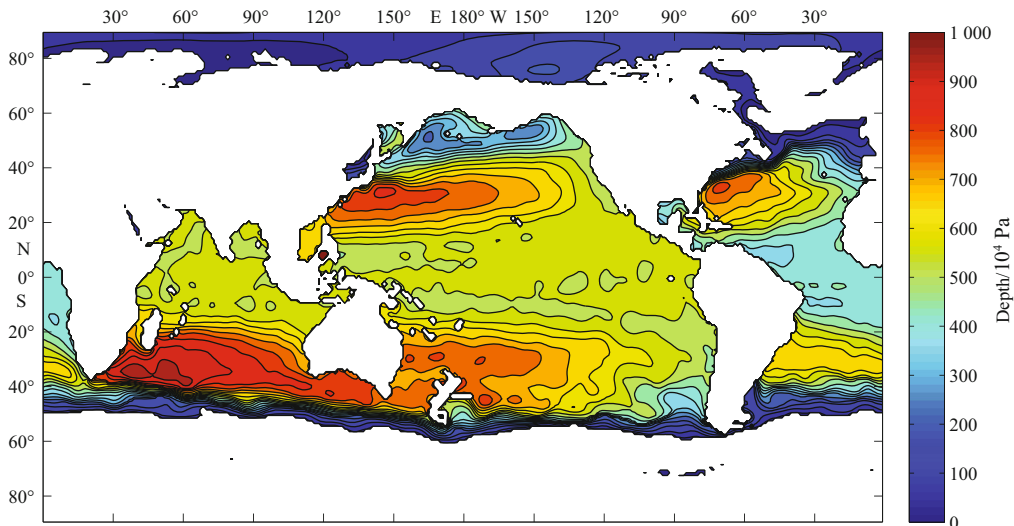


Fig.10. Depth of PDS $\sigma_{0.5}=29.3\text{kg/m}^3$.

On a PDS, thermohaline processes must depend on something other than the density, and both the spicity and elasticity may provide such additional information. The distribution of both potential temperature and salinity on the $\sigma_{0.5}=29.3 \text{ kg/m}^3$ surface gradients in the North Atlantic and North Pacific basins, Figs 11 and 12. The comparison of these two basins indicates a strong contrast of thermohaline property difference between the North Pacific Ocean and North Atlantic Ocean. It is well-known that there is strong meridional overturning circulation and deep water formation in the Atlantic Ocean. On the other hand, there is no deep water formation in the North Pacific Ocean, and the corresponding meridional overturning circulation there is very weak, if there is any. The difference in thermohaline circulation is reflected in water mass properties. The North Atlantic Ocean is characterized by warm and salty water, while the North Pacific Ocean is characterized by cold

and fresh water.

In Fig. 11, there is clearly a strong thermal front near 60°N in the Atlantic Ocean. As discussed above, such a strong thermal front may lead to a strong sink of GPE due to cabbeling associated with isopycnal diffusion. If a potential density surface is plotted for a shallower depth, the strong thermal front near 40°N associated with the Gulf Stream and Kuroshio can be seen more clearly; and such strong thermal fronts are associated with strong sink of GPE due to cabbeling associated with isopycnal diffusion.

Figure 11 clearly shows that the thermal gradient in the Atlantic Ocean is much stronger than the Pacific Ocean. As a result, GPE release due to cabbeling associated with isopycnal diffusion in the Atlantic Ocean is stronger than the Pacific Ocean. This phenomenon will be discussed in this study.

Most importantly, there are very strong fronts of temperature and salinity near the southern edge of these maps. The

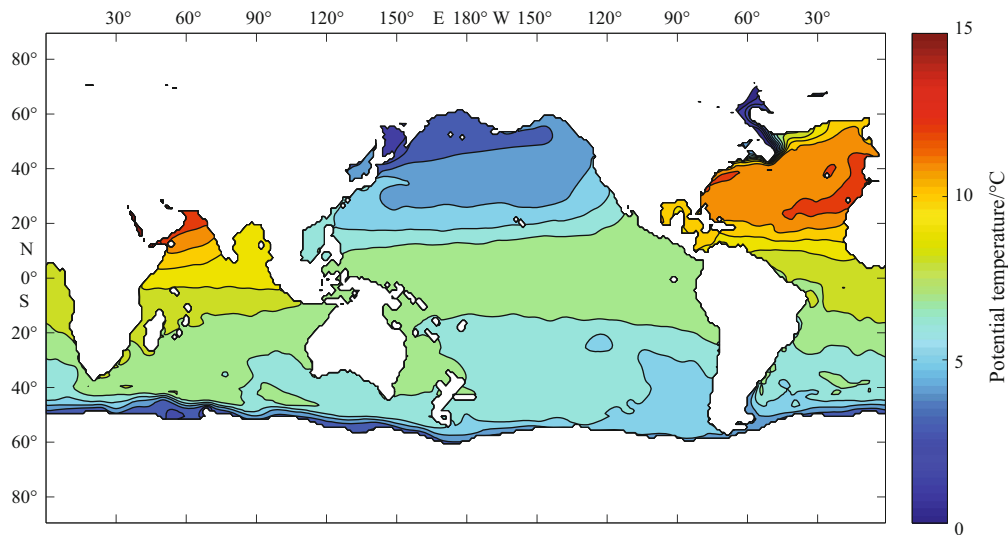


Fig.11. Potential temperature distribution on PDS $\sigma_{0.5}=29.3 \text{ kg/m}^3$.

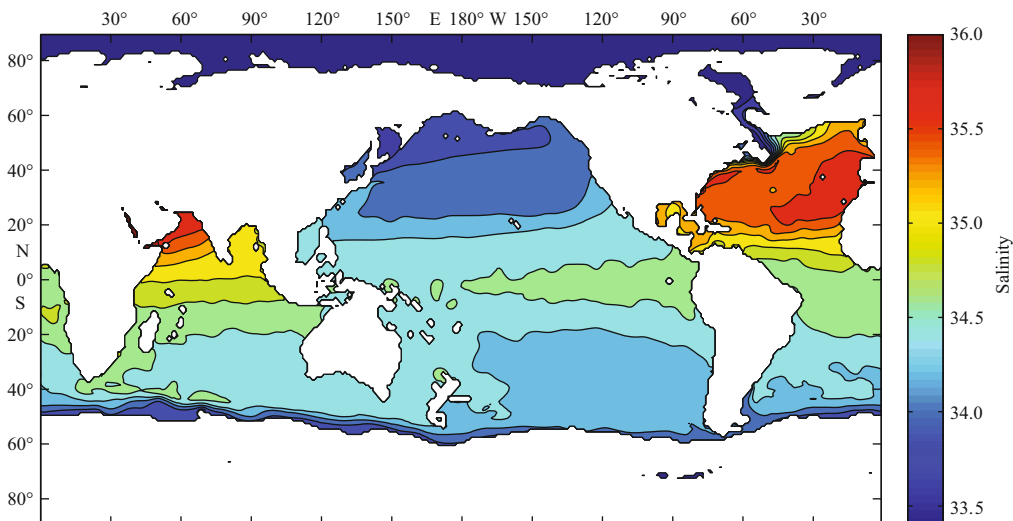


Fig.12. Salinity distribution on PDS $\sigma_{0.5}=29.3 \text{ kg/m}^3$.

slope of this surface is very steep in the Southern Ocean, and these fronts appear in the form of a rather narrow band along the southern edge of these maps. The fronts make a large contribution to GPE sink due to cabbeling associated with isopycnal diffusion, as will be discussed in the subsequently parts of this study.

The great difference in potential temperature and salinity in these two basins gives rise to remarkable differences in spicity and elasticity, as shown in Figs 13 and 14. High value of spicity in the North Atlantic Ocean has been linked to strong salt finger activity there. Negative spicity in the North Pacific Ocean and the Arctic Ocean means very little salt finger activity and the possibility of diffusive layering. However, the meaning of large horizontal gradient of spicity on this quasi-horizontal surface has not been explored, and thus it remains unclear.

We are now focused on the potential role of strong gradient

of elasticity in ACC, the North Atlantic Ocean and North Pacific Ocean (Fig. 14). The difference in elasticity over the world oceans has been linked to the selection and fate of deep water formation. Elasticity in the North Atlantic Ocean is small, on the order of 4.3 kg/m^3 , so that water there is less compressible. However, along the southern edge of the Southern Oceans, elasticity is higher than 4.6 kg/m^3 , so that deep water formed along the edge of the Antarctic Continent is most compressible. As a result, at the sea surface source of deep water formed along the southern edge of the Southern Oceans becomes the heaviest water and sink to the bottom of the world oceans. On the other hand, dense water formed in the Mediterranean Sea is less compressible. As a result, it cannot sink to the bottom of the world oceans, although its density is the highest among all source waters formed at the sea surface.

This classical example is an application of elasticity on the

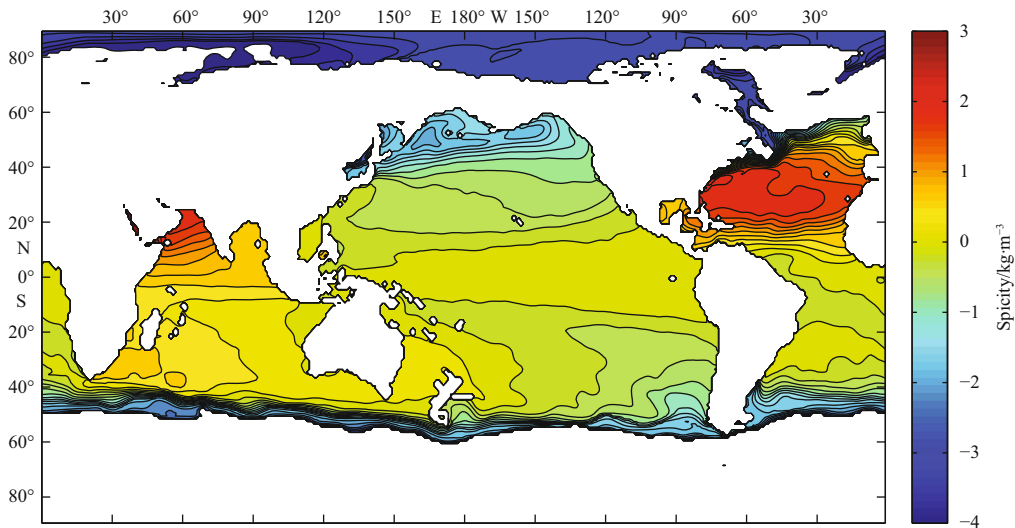


Fig.13. Spicity distribution on PDS $\sigma_{0.5}=29.3 \text{ kg/m}^3$.

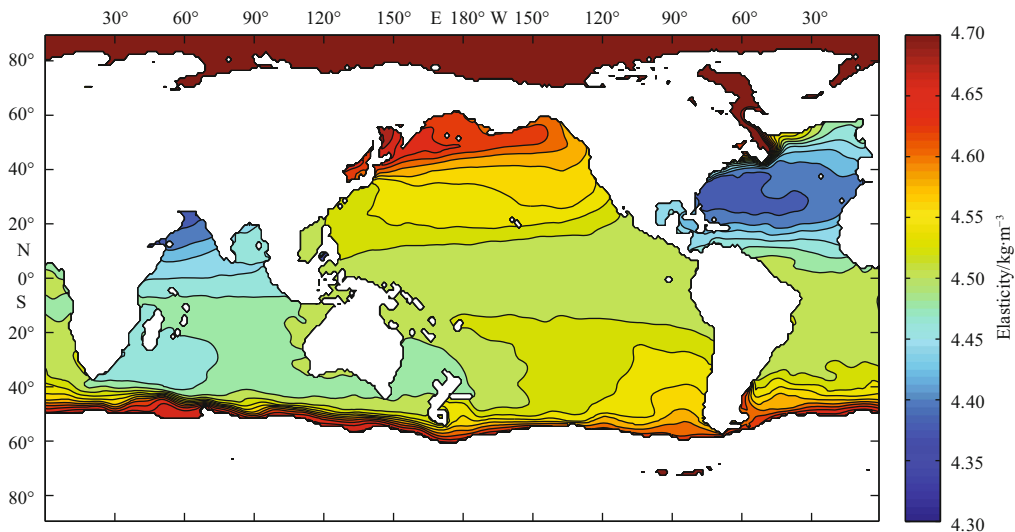


Fig.14. Elasticity distribution on PDS $\sigma_{0.5}=29.3 \text{ kg/m}^3$.

grand pole-pole scale, directly relevant to deep/bottom water formation and thermohaline circulation in the world oceans. A vitally important question is whether the gradient of elasticity can play certain roles in regulating quasi-horizontal eddy diffusion of temperature and salinity, on a horizontal scale of 1–100 km. As will be shown in Part II (Huang, 2014a), strong gradient of elasticity may be linked to the GPE release associated with isopycnal diffusion and a new type of instability, the thermobaric instability.

3 Energetics of vertical eddy diffusion

Vertical eddy diffusion is a key part of the global thermohaline circulation. According to the new paradigm of oceanic general circulation, thermohaline circulation is maintained by external sources of mechanical energy, including tidal dissipation and wind stress energy input to surface geostrophic currents. Therefore, vertical diffusivity parameterization must be constrained by the mechanical energy available. One of the key issues is how much external source of mechanical energy is available for sustaining vertical eddy diffusion, or how much GPE vertical eddy diffusion can create.

Many important questions remain open. First of all, vertical eddy diffusivity is highly non-uniform in space and time. Despite much effort in observing the rate of vertical diffusion and theoretically analyzing the rate, our understanding of vertical eddy diffusion is far from being adequate. With this uncertainty in the vertical diffusivity, we have no reliable estimate of the GPE source/sink due to vertical eddy diffusion. Nevertheless, our understanding of vertical eddy diffusion is much better than that of lateral diffusion; thus, examination of energetics of vertical diffusion can provide us a benchmark for the energetics of lateral diffusion.

In this section, we will examine how much GPE is changed due to vertical eddy diffusion. In order to closely track the change of energy, we will conceptually separate vertical eddy diffusion into two steps: stirring and subscale diffusion. During the first step, stirring, water parcels from two adjacent grids in a water column are exchanged through eddy/turbulence movements. This process of exchange is idealized as adiabatic and without change of the salinity content of each parcel. As shown in Fig. 15a, the water parcels (a2, b2) in the right half of the water column have the same mass; they exchange their positions and arrive at the new vertical locations shown in Fig. 15b. Because of the compressibility, water parcels should have a new density when they arrive at the new locations (depth), as shown schematically in Fig. 15b. Due to thermobaricity the total thickness of these two water parcels may change, as depicted by the distance between the dashed horizontal line and the solid horizontal line on the top of the water column (Fig. 15b). During this exchange, each part of this water column moves vertically. As result, the total GPE of the system is changed, and this change is counted as GPE change due to stirring associated with vertical eddy diffusion.

At the second stage, water parcels on the same box level are mixed through subscale diffusion, i.e., a1 and b2 are mixed and a new water parcel a1b2 is produced; similarly, b1 and a2 are mixed and a new water parcel b1a2 is produced. Due to cabeling, the density of the newly formed water parcels is higher than the mean of the parents parcels; thus, there are GPE loss associated with the subscale diffusion. Note that in this study,

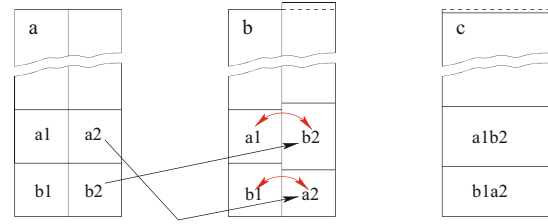


Fig.15. Separating vertical eddy diffusion into two steps: stirring and subscale diffusion. The dashe lines on the top are the original sea surface, and the solid lines are the new sea surface after stirring or subscale diffusion. a. Initial state, b. After stirring, and c. After subscale diffusion.

we will use eddy diffusion to describe tracer diffusion processes on spatial scale much larger than the molecular level. For this purpose, we will reserve the term “mixing” and use an alternative name “subscale diffusion” for the second stage.

3.1 Gravitational potential energy change due to vertical stirring

Change in concentration of a tracer C can be described in terms of the tracer balance equation, and in pressure coordinate, this can be written in the following form

$$\frac{\partial C}{\partial t} + \bar{U} \cdot \nabla_3 C = \nabla_p \cdot (K \nabla_p C) + \frac{\partial}{\partial p} \left(\kappa_p \frac{\partial C}{\partial p} \right), \quad (12)$$

where \bar{U} is the 3-dimensional velocity, pressure is used as the vertical coordinate, ∇_3 is a 3-dimensional operator, ∇_p is the 2D horizontal operator in pressure coordinates, K is the horizontal diffusivity, κ_p is the vertical diffusivity in unit of Pa^2/s . Note that the 3-dimensional velocity can be treated in terms of the large-scale mean velocity plus the eddy transport term, i.e., $\bar{U} = \bar{u} + u'$. Eddy transport has been discussed in many previous studies, such as Gent and McWilliams (1990) and Gent et al. (1995). One of the most important assumptions made in the derivation of eddy transport is that density is a linear function of potential temperature and salinity. In this study, we will explore the consequence of nonlinear equation of state of seawater.

Since our focus in this section is the consequence of vertical eddy diffusion, we will temporally omit the advection terms and the horizontal diffusion term, i.e. we will be concentrated on the contribution due to vertical eddy diffusion alone, and Eq. (12) is reduced to the following equation

$$\frac{\partial C}{\partial t} = \frac{\partial}{\partial p} \left(\kappa_p \frac{\partial C}{\partial p} \right). \quad (13)$$

The first step is to analyze GPE change due to the vertical stirring of water masses. We will ignore the effect of double diffusion, i.e. the different diffusion characters associated with the two major components of seawater, salinity and temperature. Instead, we will assume vertical eddy diffusivity is the same for both temperature and salinity.

In the following analysis we will temporally assume that vertical diffusivity κ_p is constant in space and time. For a grid box

of finite size Δp_k , the differential Eq. (13) can be converted into the following form

$$\Delta p_k \frac{\partial C_{i,j,k}}{\partial t} = \kappa_p \left[\left(\frac{\partial C}{\partial p} \right)^+ - \left(\frac{\partial C}{\partial p} \right)^- \right], \quad (14)$$

where $(\partial C / \partial p)^+$ and $(\partial C / \partial p)^-$ are the tracer gradient at the lower (higher pressure) and upper (lower pressure) boundaries of this grid box. Applying this equation to water density leads to the following equation

$$\Delta p_k \frac{\partial \rho_{i,j,k}}{\partial t} = \kappa_p \times \left[\frac{2}{\Delta p_k + \Delta p_{k-1}} (\rho'_{i,j,k-1} - \rho_{i,j,k}) + \frac{2}{\Delta p_k + \Delta p_{k+1}} (\rho'_{i,j,k+1} - \rho_{i,j,k}) \right], \quad (15)$$

where $\rho'_{i,j,k-1}$ and $\rho'_{i,j,k+1}$ are the new *in-situ* density water parcels from grid $(i, j, k-1)$ and $(i, j, k+1)$ obtained after they adiabatically arrive at the new *in-situ* pressure of p_k . Note that the new density labeled by primes should be calculated as potential density, using p_k as the reference pressure.

This equation can be rewritten in a slightly different form

$$\Delta p_k \frac{1}{\rho_{i,j,k}} \frac{\partial \rho_{i,j,k}}{\partial t} = \kappa_p \times \left[\frac{2}{\Delta p_k + \Delta p_{k-1}} \left(\frac{\rho'_{i,j,k-1}}{\rho_{i,j,k}} - 1 \right) + \frac{2}{\Delta p_k + \Delta p_{k+1}} \left(\frac{\rho'_{i,j,k+1}}{\rho_{i,j,k}} - 1 \right) \right], \quad (15')$$

Density change in a grid box is linked to the GPE for the whole water column above this water parcel at this station. Due to the change of density a water parcel's volume increases (or declines). If the density change of a water parcel with thickness $\Delta h_{i,j,k}$ is $\delta \rho_{i,j,k}$, its height change is

$$\delta h_{i,j,k} = -\Delta h_{i,j,k} \delta \rho_{i,j,k} / \bar{\rho}, \quad (16)$$

where $\bar{\rho}$ is the mean reference density. As a result, the whole water column above must be moved upward (or down, depending on the sign of density change) over a vertical distance $\delta h_{i,j,k}$. Assume the water parcel has a horizontal area A_S , the increment of the total GPE of the water column above is

$$\delta \chi = p_k A_S \delta h_{i,j,k} = -p_k A_S \Delta h_{i,j,k} \delta \rho_{i,j,k} / \bar{\rho}, \quad (17)$$

where p_k is the *in-situ* pressure at the center of this water parcel, which remains unchanged because we use the pressure coordinates and exchange water parcels with equal mass. Note that we omit the contribution associated with the vertical migration of the center of mass of the water parcel itself because this is a higher order term, which is small and negligible.

Using Eq. (15'), the rate of GPE change per unit area associated with vertical stirring is

$$\dot{\chi}_{\text{stir}}^{\text{vert,diffu}} = C \kappa_p \frac{p_k}{g \bar{\rho}} \times \left[\frac{2}{\Delta p_k + \Delta p_{k+1}} \left(1 - \frac{\rho'_{i,j,k+1}}{\rho_{i,j,k}} \right) + \frac{2}{\Delta p_k + \Delta p_{k-1}} \left(1 - \frac{\rho'_{i,j,k-1}}{\rho_{i,j,k}} \right) \right], \quad (18)$$

Note that in common practice, pressure in unit of 10^4 Pa is used; thus, this formula includes an additional factor of $C=10000$ for unit conversion.

For the lowest grid above the sea floor, there is no diffusion across the bottom boundary, so that the corresponding formula is

$$\dot{\chi}_{\text{stir}}^{\text{vert,diffu}} = C \kappa_p \frac{1}{g \bar{\rho}} \frac{2 p_k}{\Delta p_k + \Delta p_{k-1}} \left(1 - \frac{\rho'_{i,j,k-1}}{\rho_{i,j,k}} \right). \quad (18')$$

Since potential density increases with depth in general, $\rho'_{i,j,k-1} < \rho_{i,j,k}$, i.e. water in the lowest grid expands due to vertical stirring. Therefore, GPE due to diffusion in the lowest grid is always increased. Similarly, GPE change for the box on the sea surface can be derived.

Assuming that the grid thickness is equal, Eq. (18) is reduced to

$$\begin{aligned} \dot{\chi}_{\text{stir}}^{\text{vert,diffu}} &= C \kappa_p \frac{p_k}{g \bar{\rho} \Delta p_k} \left[2 - (\rho'_{i,j,k-1} + \rho'_{i,j,k+1}) / \rho_{i,j,k} \right] \\ &\approx C \kappa_p \frac{h_k}{\Delta p_k} \left[2 - (\rho'_{i,j,k-1} + \rho'_{i,j,k+1}) / \rho_{i,j,k} \right]. \end{aligned} \quad (19)$$

3.2 Gravitational potential energy change due to cabbeling associated with vertical subscale diffusion

Due to vertical stirring, temperature at a grid box also changes. Similar to Eq. (15), thus, over a time interval of Δt , the temperature perturbation induced by vertical exchange of water mass is

$$\Delta T_{i,j,k} = B \left[\frac{2}{\Delta p_k + \Delta p_{k-1}} (\Theta_a - T_{i,j,k}) + \frac{2}{\Delta p_k + \Delta p_{k+1}} (\Theta_b - T_{i,j,k}) \right], \quad (20)$$

$$B = \frac{\kappa_p \Delta t}{\Delta p_k}, \quad (21)$$

where Θ_a and Θ_b are potential temperature of water coming from above and below. Thus, after a time interval of

$$\Delta \tau = \frac{\Delta p_k}{\kappa_p D_k}, \quad D_k = \frac{2}{\Delta p_k + \Delta p_{k-1}} + \frac{2}{\Delta p_k + \Delta p_{k+1}}, \quad (22)$$

at grid point (i, j, k) the new potential temperature, salinity and density are

$$\bar{T}_{i,j,k} = T_{i,j,k} + \Delta T_{i,j,k} = \left[\frac{2}{\Delta p_k + \Delta p_{k-1}} \Theta_a + \frac{2}{\Delta p_k + \Delta p_{k+1}} \Theta_b \right] D_k^{-1}, \quad (23)$$

$$\bar{S}_{i,j,k} = S_{i,j,k} + \Delta S_{i,j,k} = \left[\frac{2}{\Delta p_k + \Delta p_{k-1}} S_a + \frac{2}{\Delta p_k + \Delta p_{k+1}} S_b \right] D_k^{-1}, \quad (24)$$

$$\bar{\rho}_{i,j,k} = \rho_{i,j,k} + \Delta \rho_{i,j,k} = \left[\frac{2}{\Delta p_k + \Delta p_{k-1}} \rho'_a + \frac{2}{\Delta p_k + \Delta p_{k+1}} \rho'_b \right] D_k^{-1}, \quad (25)$$

where S_a, ρ'_a are salinity and potential density of water coming from the cell above, and S_b, ρ'_b are salinity and potential density of water coming from the cell below.

For the last grid above the seafloor, diffusion takes place between water from above and water originally in the cell.

$$\Delta T_{i,j,k} = B \frac{2}{\Delta p_k + \Delta p_{k-1}} (\Theta_a - T_{i,j,k}), \quad (26)$$

$$B = \frac{\kappa_p \Delta t}{\Delta p_k}. \quad (27)$$

After a time interval of

$$\Delta \tau = \frac{\Delta p_k}{\kappa_p D_{kb}}, \quad D_{kb} = \frac{2}{\Delta p_k + \Delta p_{k-1}}, \quad (28)$$

thus, the new potential temperature, salinity and density at the end of this time interval are

$$\bar{T}_{i,j,k} = T_{i,j,k} + \Delta T_{i,j,k} = 0.5(\Theta_a + T_{i,j,k}), \quad (29)$$

$$\bar{S}_{i,j,k} = S_{i,j,k} + \Delta S_{i,j,k} = 0.5(S_a + S_{i,j,k}), \quad (30)$$

$$\bar{\rho}_{i,j,k} = \rho_{i,j,k} + \Delta \rho_{i,j,k} = 0.5(\rho'_a + \rho_{i,j,k}). \quad (31)$$

The new density after subscale diffusion is

$$\rho_{i,j,k,\text{mix}} = \rho(\bar{S}_{i,j,k}, \bar{T}_{i,j,k}, p_k). \quad (32)$$

The total change of GPE of this water column can be calculated as

$$\Delta \chi_{\text{cabb}}^{\text{vert,diffu}} = p_k \delta \Delta h_{i,j,k} \Delta x_j \Delta y = p_k (\bar{\rho}_{i,j,k} / \rho_{i,j,k,\text{mix}} - 1) \Delta h_{i,j,k} \Delta x_j \Delta y. \quad (33)$$

Thus, over the time period of $\Delta \tau$ the mean rate of GPE change per unit horizontal area is

$$\begin{aligned} \dot{\chi}_{\text{cabb}}^{\text{vert,diffu}} &= p_k (\bar{\rho}_{i,j,k} / \rho_{i,j,k,\text{mix}} - 1) \Delta h_{i,j,k} / \Delta \tau \\ &= \kappa_p p_k (\bar{\rho}_{i,j,k} / \rho_{i,j,k,\text{mix}} - 1) D_k \Delta h_{i,j,k} / \Delta p_k \\ &\approx C \kappa_p h_k (\bar{\rho}_{i,j,k} / \rho_{i,j,k,\text{mix}} - 1) D_k. \end{aligned} \quad (34)$$

3.3 Application to the world oceans

As discussed in Section 1, our analysis in this section will be based on the WOA01 data converted to the pressure coordinate. The GPE change formulae discussed above are applied to the world oceans, with 1° horizontal resolution and 33 layers in the vertical direction. Vertical eddy diffusivity in the ocean has been discussed in many previous studies. In a classical paper by Munk (1966), the world ocean mean density profiles were fitted to a one-dimensional advection and diffusion balance equation. The bulk vertical eddy diffusivity was estimated at a classical value of $10^{-4} \text{ m}^2/\text{s}$. *In-situ* measurements, however, indicate that vertical eddy diffusivity in the ocean interior away from boundaries is about 10 times smaller (Ledwell et al., 1993).

On the other hand, vertical eddy diffusivity near the mid-ocean ridge can be as high as 20 times of the mean bulk value of $10^{-4} \text{ m}^2/\text{s}$ inferred by Munk (Ledwell et al., 2000). There have been great wealth of data collected from the ocean, which present a complicated pattern of diffusivity. However, in this study, we will limit our discussion for the case with uniform vertical eddy diffusivity. Since we will use the pressure coordinates, with the commonly used pressure unit in 10^4 Pa , the corresponding value of vertical eddy diffusivity is set to $\kappa_p = 2 \times 10^3 \text{ Pa}^2/\text{s}$.

The vertical distribution of GPE source/sink due to vertical eddy stirring is shown in Fig. 16. Since vertical stirring pushes cold water upward and warm water downward, vertical eddy stirring increases the GPE of the system in general. On the other hand, cabbeling associated with subscale diffusion always leads to loss of GPE. Therefore, source of GPE is due to stirring and sink of GPE is due to cabbeling. For the GPE source, there are three peaks: the first one in the depth of $200 \times 10^4 - 300 \times 10^4 \text{ Pa}$, the second one in the depth range of $2000 \times 10^4 - 2500 \times 10^4 \text{ Pa}$, and the third one in the depth range of $4000 \times 10^4 - 4500 \times 10^4 \text{ Pa}$. On the other hand, cabbeling lost of GPE is maximal in the upper $500 \times 10^4 \text{ Pa}$, and there is very small loss of GPE below this

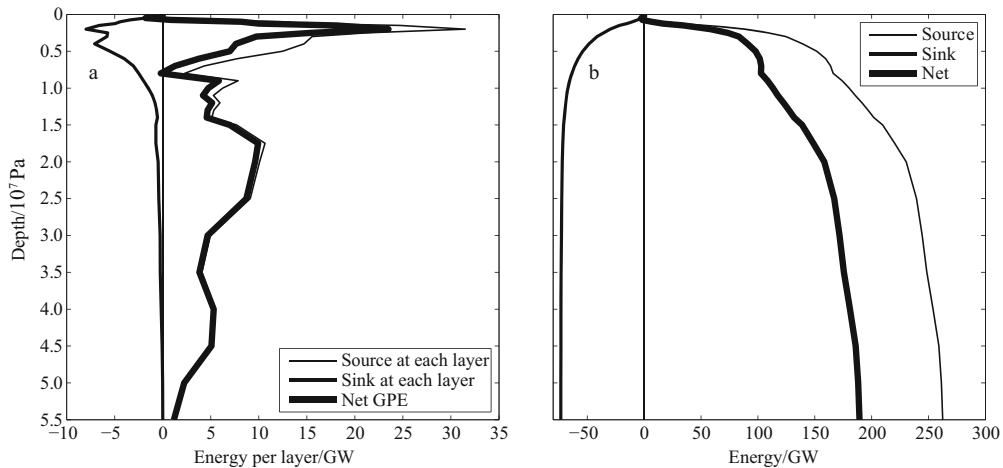


Fig.16. Vertical distribution of GPE source and sink in the world oceans due to vertical stirring and subscale diffusion. a. Source/sink distribution, and b. Accumulated sour/sink.

depth range.

The total source of GPE due to vertical stirring is estimated at 263 GW, and the total loss of GPE due to cabbeling is estimated at 73 GW; thus, the net increase of GPE associated with vertical diffusion in the world oceans is estimated at 189 GW. Note that cabbeling works against the GPE creation by vertical diffusion. For the parameter used in this study, cabbeling loss of GPE consists of 28% of the GPE created by vertical stirring. Were the equation of state linear, such loss of GPE due to cabbeling would not exist.

The meridional distribution of GPE source/sink is shown in Fig. 17a. It is clear that high source/sink is located at low latitudes, which is closely linked to the fact that stratification at low latitudes is much higher than at high latitudes. In addition, there is slight bias towards the Northern Hemisphere, which is again likely to be linked to the difference in the mean stratification. The three peaks of source/sink in the zonal distribution of

GPE source/sink are closely linked to geometry of three basins, as shown in Fig. 17b.

The horizontal maps of GPE source/sink and the net gain are shown in Figs 18, 19 and 20. The regions of high rate of GPE source and sink at low latitudes, in particular the warm pool, are clearly linked to the strong stratification in these areas. The global source maximum is in the Bay of Bengal, which is apparently linked to the strong stratification associated with freshwater flux from the land.

The GPE sink maximum is located in the middle of equatorial Pacific. An interesting phenomenon is that along the eastern boundaries of the Pacific and Atlantic there are bands of relatively low rate of GPE loss due to cabbeling (Fig. 19). These bands of low rate of GPE sink may be closely linked to the upwelling systems in these regions. In addition, the whole ACC system appears as a band of low GPE loss, which is likely due to the strong upwelling there. However, the detail analysis is left

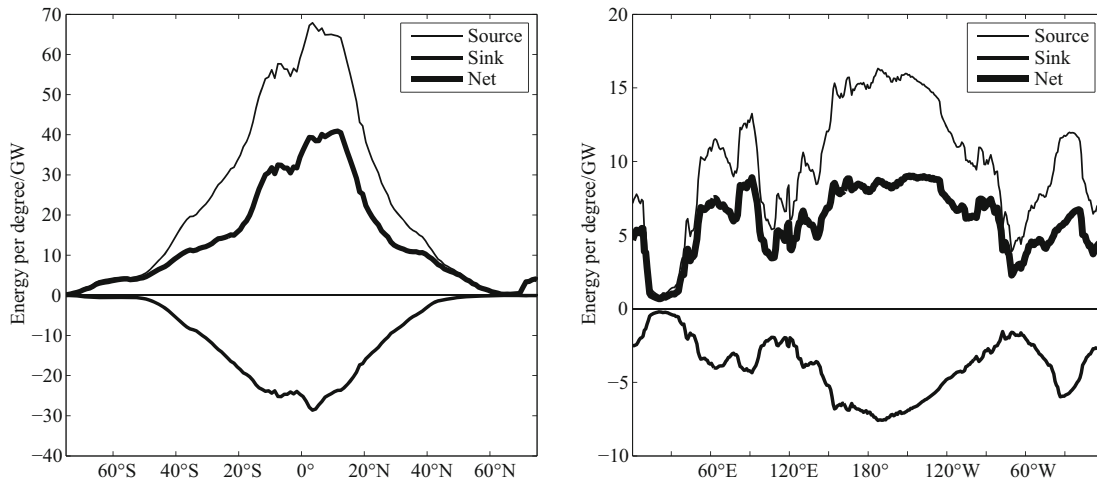


Fig.17. Meridional and zonal distributions of GPE source/sink in the world oceans due to vertical stirring and subscale diffusion. a. Meridional GPE due to vertical stirring/cabbeling, b. zonal GPE due to vertical stirring/cabbeling.

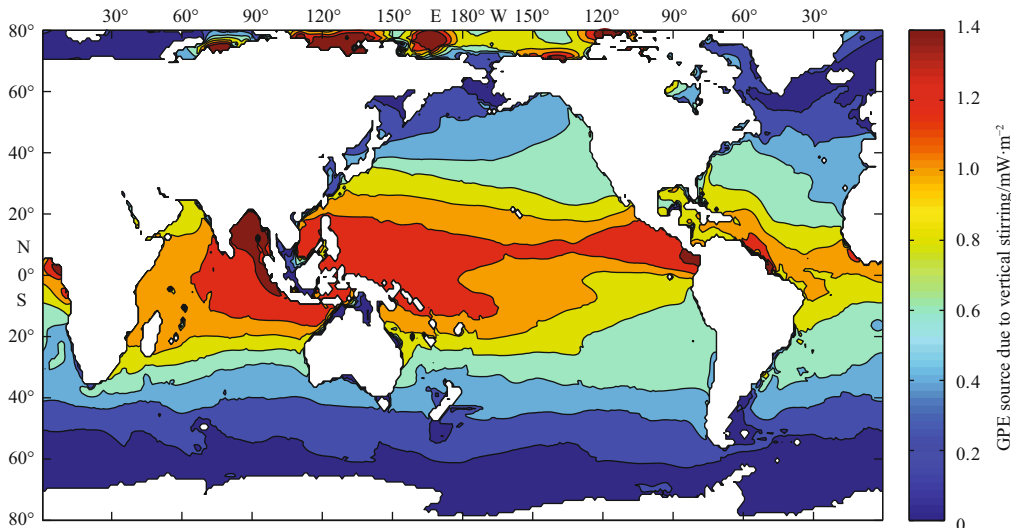


Fig.18. Horizontal distribution of GPE source in the world oceans due to vertical stirring.

for further study.

The combination of GPE source and sink gives rise to a map shown in Fig. 20. The most unique feature of this map is the two areas of strong net GPE gain due to vertical diffusion: the cold tongue in the equatorial east Pacific Ocean and the warm water pool in the western equatorial Pacific Ocean and the closely linked part of the equatorial Indian Ocean. The northern end of the Bay of Bengal appears as the site of maximum net GPE gain.

3.4 Remark

Gravitational potential energy change associated with vertical eddy diffusion is discussed. Since we still do not know the exact spatial distribution of vertical eddy diffusivity well enough, we assume that the vertical eddy diffusivity is equal to a constant value of $2 \times 10^3 \text{ Pa}^2/\text{s}$, which is equivalent to a value of $2 \times 10^{-5} \text{ m}^2/\text{s}$ for the z -coordinate. For the world oceans, the total

amount of GPE increase due to vertical stirring is estimated at 263 GW. Cabbeling associated with vertical diffusion is a sink of GPE, and the total value of energy lost is estimated at 73 GW. Thus, the net source of GPE is estimated at 189 GW.

Since the formulae for calculating GPE source/sink is linearly dependent on the verticals eddy diffusivity, one can use such formulae to calculate the corresponding GPE source/sink for any constant diffusivity. Assuming the classical value of $\kappa_p = 2 \times 10^3 \text{ Pa}^2/\text{s}$ recommended by Munk (1966) would give rise to a big rate of GPE source due to vertical eddy diffusion, on the order of 1 TW. Tidal dissipation in the open ocean is on the order of 0.7–0.9 TW (Munk and Wunsch, 1998); assuming a conversion efficiency of 0.2, we estimate the upper bound of the external source due to tidal mixing is 0.18 TW. Thus, the classical value of Munk (1966) is too high, and a much smaller value should be used in models.

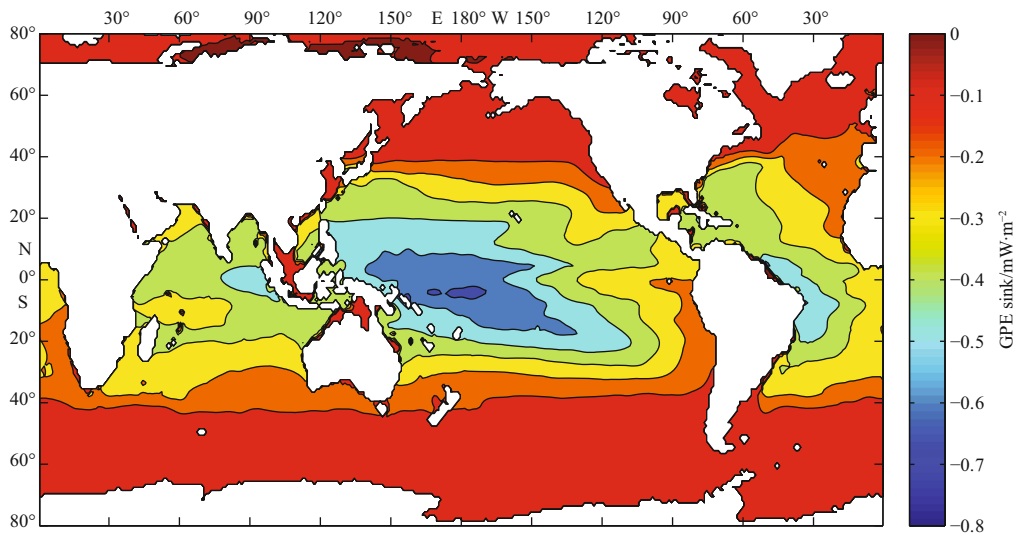


Fig.19. Horizontal distribution of GPE sink in the world oceans due to cabbeling associated with vertical subscale diffusion.

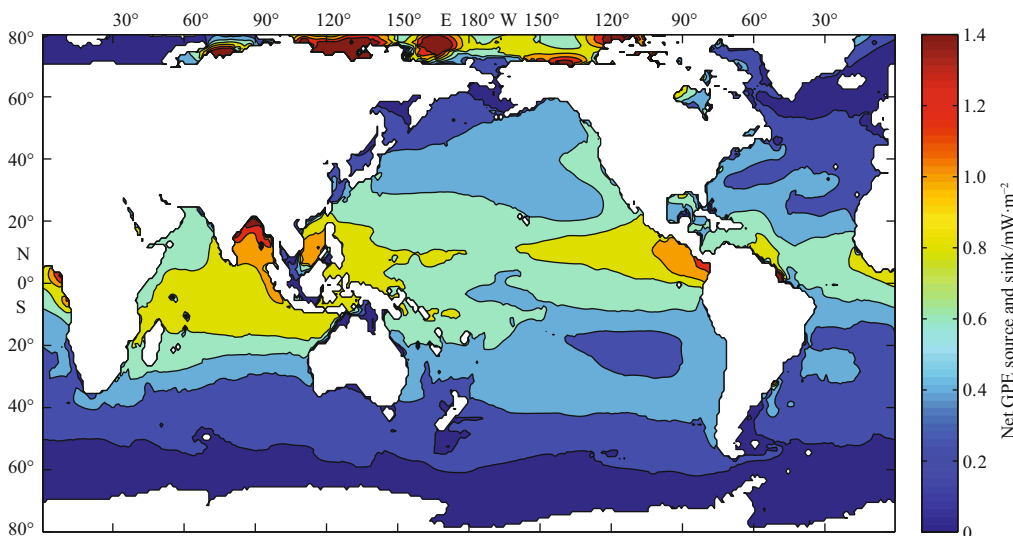


Fig.20. Horizontal distribution of net GPE source/sink in the world oceans due to vertical stirring and subscale diffusion.

Calculation shown above is simple and quite straightforward, and the results are within the range of expected values. It is to remind the reader that the simple GPE source/sink patterns shown in Figs 18, 19 and 20 is the logical consequence of assuming a globally constant vertical eddy diffusivity. Instead of inferring the source and sink of GPE in the world ocean by assuming the vertical eddy diffusivity, the distribution of GPE source and sink should be directly linked to the external source of mechanical energy available for sustaining vertical eddy mixing. In other words, the energy diagram shown in Fig. 1 should be expanded into a two-dimensional distribution map. However, such a map is beyond the scope of this study.

The reason to include such a simple calculation is to demonstrate the basic idea of how to use the energy available for mixing as an integral constraint. In fact, over the past two decades, it is an important step forward in subgrid scale parameterization. In the rest of this study, we will gradually move forward, using the source/sink of GPE associated with lateral diffusion and advection diagnosed from numerical models as a benchmark to evaluate how well does a model simulate the physics of the ocean circulation in terms of GPE balance.

Acknowledgements

This study took more than three years to finish. During this long period of time, I received persistent encouragement from many of my colleagues. In particular, discussing seawater thermodynamics with Ray Schmitt has always been a great pleasure; Yihua Lin provided very stimulating discussion about thermobaric instability; Quanan Zheng provided the most need support and suggestions, and I take this opportunity to thank all my colleagues who gave the most needed support.

References

- Carton J A, Giese B S. 2008. A reanalysis of ocean climate using simple ocean data assimilation (SODA). *Mon Weather Rev*, 136: 2999–3017
- Conkright M E, Locarnini R A, Garcia H E, et al. 2002. World Ocean Atlas 2001: Objective Analysis, Data Statistics, and Figures. CD-ROM Documentation, National Oceanographic Data Center, Silver Spring, MD, 17
- Eden C, Willebrand J. 1999. Neutral density revisited. *Deep-Sea Res Pt II*, 46: 33–54
- Feistel R. 1993. Equilibrium thermodynamics of seawater revisited. *Prog Oceanogr*, 31: 101–179
- Flament P. 2002. A state variable for characterizing water masses and their diffusive stability: spiciness. *Progr Oceanogr*, 54: 493–501
- Fofonoff N P. 1998. Nonlinear limits to ocean thermal structure. *J Mar Res*, 56: 793–811
- Fofonoff N P. 2001. Thermal stability of the world ocean thermoclines. *J Phys Oceanogr*, 31: 2169–2177
- Gent P R, Willebrand J, McDougall T J, et al. 1995. Parameterizing eddy-induced tracer transports in ocean circulation models. *J Phys Oceanogr*, 25: 463–474
- Gent P R, McWilliams J C. 1990. Isopycnal mixing in ocean circulation models. *J Phys Oceanogr*, 20: 150–155
- Gill A E. 1973. Circulation and bottom water production in the Weddell Sea. *Deep Sea Res*, 20: 111–140
- Griffies S M, Pacanowski R C, Hallberg R W. 2000. Spurious diapycnal mixing associated with advection in a z-coordinate ocean model. *Monthly Weather Review*, 128: 538–564
- Huang R X. 1999. Mixing and energetics of the thermohaline circulation. *J Phys Oceanogr*, 29: 727–746
- Huang R X. 2010. Ocean Circulation, Wind-driven and Thermohaline Processes. Cambridge, United Kingdom: Cambridge University Press, 806
- Huang R X. 2011. Defining the spicity. *J Mar Res*, 69: 1–15
- Huang R X. 2014a. Energetics of lateral eddy diffusion/advection: Part II. Numerical diffusion/diffusivity and gravitational potential energy change due to isopycnal diffusion. *Acta Oceanol Sin*, 33(3): 19–39
- Huang R X. 2014b. Energetics of lateral eddy diffusion/advection: Part III. Energetics of horizontal and isopycnal diffusion/advection. *Acta Oceanol Sin*, 33(3): 40–57
- Huang R X. 2014c. Energetics of lateral eddy diffusion/advection: Part IV. Energetics of diffusion/advection in sigma coordinates and other coordinates. *Acta Oceanol Sin*, 33(3): 58–81
- Jackett D R, McDougall T J. 1997. A neutral density variable for the world's oceans. *J Phys Oceanogr*, 27: 237–263
- Ledwell J R, Montgomery E T, Polzin K L, et al. 2000. Evidence for enhanced mixing over rough topography in the abyssal ocean. *Nature*, 403: 179–182
- Ledwell J R, Watson A J, Law C B. 1993. Evidence for slow mixing across the pycnocline from an open-ocean tracer-release experiment. *Nature*, 364: 701–703
- Munk W H. 1966. Abyssal recipes. *Deep-Sea Res*, 13: 707–730
- Munk W H. 1981. Internal waves and small-scale processes. In: *Evolution of Physical Oceanography*, Cambridge, MA: MIT Press, 264–291
- Munk W H, Wunsch C. 1998. Abyssal recipes II: energetics of the tidal and wind mixing. *Deep-Sea Res Pt I*, 45: 1977–2010
- Price J F, Baringer M O. 1994. Outflows and deep water production by marginal seas. *Progr Oceanogr*, 33: 161–200
- Ruddick B, Kerr O. 2003. Oceanic thermohaline intrusions: theory. *Progr Oceanogr*, 56: 483–497
- Ruddick B, Richards K. 2003. Oceanic thermohaline intrusions: observations. *Progr Oceanogr*, 56: 499–527
- Stommel H. 1962. On the cause of the temperature-salinity curve in the ocean. *Proceedings of the National Academy of Science USA*, 48: 764–766
- Veronis G. 1972. On properties of seawater defined by temperature, salinity and pressure. *J Mar Res*, 30: 227–255